Data in Brief 57 (2024) 110988

Contents lists available at ScienceDirect

Data in Brief

journal homepage: www.elsevier.com/locate/dib

Data Article

Data pertaining to the catalytic capabilities of transition metal oxides for fuel cell applications

Salaminah Bonolo Boshoman, Olawale Samuel Fatoba*

Department of Mechanical Engineering Science, University of Johannesburg, Johannesburg, South Africa

ARTICLE INFO

Article history:
Received 12 June 2024
Revised 15 August 2024
Accepted 25 September 2024
Available online 3 October 2024

Dataset link: Data Related to the Catalytic Capabilities of Transition Metal Oxides for Energy Applications (Original data)

Keywords:
Transition metal oxides
Computational studies
Nanostructured oxides
Electrocatalysts
Fuel cells
Density functional theory

ABSTRACT

The burning of fossil fuels produces pollutants and has a negative effect on the environment; however, it is still the primary source of energy for much of the globe today. This is why there has been a surge in interest in studying how to generate energy in a more environmentally friendly and long-term fashion. The widespread use of fuel cell technology—which efficiently converts electrochemical energy to electrical energy while producing almost no carbon emissions—is a prime illustration of this effort. The oxygen reduction reaction (ORR), which is utilized for catalysis inside fuel cell membranes, is slow, and platinum (Pt) is expensive and unstable, which limits the efficiency and broad application of fuel cell technology. This work investigates nanomaterials made of titanium, cobalt, and tungsten oxides as potential inexpensive and active electrocatalysts. Nanomaterials made of cobalt, tungsten, and titanium oxides have become increasingly popular as potential materials with catalytic capabilities that are both inexpensive and effective, especially when compared to conventional platinum catalysts. When used as fuel cell catalysts, the bimetallic compositions of these transition metals and oxygen have been the subject of surprisingly little theoretical and experimental investigation. Crystallographic surfaces of $CoWO_4$ (011), $CoWO_4$ (100), $CoWO_4$ (111), Co_3WO_8 (001), Co_3WO_8 (101), Co_3WO_8 (011), $TiWO_4$ (100), $TiWO_4$ (101), and $TiWO_4$ (110) are the principal focus of this investigation into their catalytic capacities. The

* Corresponding author.
E-mail address: proffatobasameni@gmail.com (O.S. Fatoba).

https://doi.org/10.1016/j.dib.2024.110988

electronic characteristics of the structures were studied using Density Functional Theory (DFT) with CASTEP and DMol3, and oxygen adsorption on the different surface configurations was done using the Adsorption Locator module.

Specifications Table

Subject	Materials science, materials chemistry
Specific subject area	Computational materials science.
Type of data	Tables, Figures. Raw, Analysed.
Data collection	The BIOVIA Material Studio software's powerful capabilities in accurately modelling materials at the molecular and atomic levels set it apart. Because of how well it uses density-functional theory calculations, the electrical characteristics and behaviours of catalyst materials may be studied in detail. The software's molecular dynamics simulation capabilities further shed light on the catalyst systems' atomic and molecular interactions and dynamic behaviour. Its ability to simplify basic-level computations and simulations can greatly aid in deciphering critical insights needed for fuel cell catalyst material innovation and optimization. Complex periodic systems can be studied using density functional theory (DFT). This greatly aids in resolving issues in materials processing and design. This section utilizes structural data from the Materials Project and DFT methods in BIOVIA Materials Studio to shed light on the underlying physics and chemistry of new transition metal oxide electrocatalysts. Here, the basic chemistry and physics of new transition metal oxide electrocatalysts are explored using density-functional theory (DFT) methods in BIOVIA Materials Studio, in conjunction with structural data from the Materials Project. In order to optimize the geometry and conduct electronic structural analysis on the $CoWO_4$, Co_3WO_8, and $TiWO_4$ structures, the CASTEP and Dmol3 modules were utilized. We investigated H_2 and O_2 adsorption on the surfaces of $CoWO_4$, Co_3WO_8, and $TiWO_4$ using the Adsorption Locator module. Based on the ideas described earlier, we use Materials Studio to model and simulate the Ti-Co-W oxide structures. BIOVIA, a company specializing in research tools for fields like computational chemistry, quantum mechanics, molecular dynamics simulations, bioinformatics, and chemoinformatics, developed and distributed the software package. The Material Studio application allows for in-depth investigations of a wide range of materials, including catalysts, polymers, nanotubes, metals, ceramics, and more. A large number of researchers have made use of this instrument to overcome obstacles in catalyst and fuel cell development. This study utilizes a number of computer modules specifically designed for material property simulations and predictive modelling. Two important modules used are DMol3, which makes predictions about material characteristics, and CASTEP, which makes predictions about electrical, optical, and structural properties and allows comparisons with DMol3. Furthermore, the Adsorption Locator module pinpoints the most stable adsorption locations on surfaces. Two more important modules are Sorption and ONETEP. Sorption predicts basic properties like sorption isotherms and Henry's constants, and ONETEP runs simulations using linear-scaling density functional theory. Drug discovery and QSAR are just two of the many applications that benefit from the VAMP's fast calculations of various molecular characteristics. Finally, QSAR Plus identifies molecules with optimum physicochemical features. When used together, these modules provide an extensive computational understanding of the behaviour and usefulness of materials in a wide range of applications [1–4].

(*continued on next page*)

	This study's computations consider many factors, including gas adsorption, state density, population analysis, band structure, electron density, and gas density. The structural and property data was retrieved using the Materials Project (MP), an invaluable resource for materials research. The data was then input into the materials design program Material Studio (Biovia 2020), which allows for the modelling of hydrogen and oxygen adsorption on surfaces of transition metal oxides, as well as shape optimization. The crude constructions that were brought in from the materials project were cut into surfaces: $CoWO_4$ (011), $CoWO_4$ (100), $CoWO_4$ (111), Co_3WO_8 (001), Co_3WO_8 (101), Co_3WO_8 (011), $TiWO_4$ (100), $TiWO_4$ (101), and $TiWO_4$ (110). A 20-Å vacuum was generated in order to replicate a realistic setting.
Data source location	Department of Mechanical Engineering Science, University of Johannesburg, South Africa.
Data accessibility	BOSHOMAN, SALAMINAH; FATOBA, OLAWALE (2024), "Data Related to the Catalytic Capabilities of Transition Metal Oxides for Energy Applications.", Mendeley Data, V1, doi: 10.17632/7w9554zbf6.1 Repository name: Mendeley Data Data identification number: doi: 10.17632/7w9554zbf6.1 Direct URL to data: https://data.mendeley.com/datasets/7w9554zbf6/1
Related research article	S.B. Boshoman, O.S. Fatoba, O.O. Dada, T.C. Jen, Transition metal oxide catalytic abilities for fuel cell applications: Density functional theory (DFT) studies, Materials Today Communications, Volume 39, 2024, 109,125, pp. 1–16. https://doi.org/10.1016/j.mtcomm.2024.109125.

1. Value of the Data

- For the first time, this study investigated a variety of surfaces for possible catalytic materials for HOR and ORR fuel cell applications, including $CoWO_4$ (011), $CoWO_4$ (100), $CoWO_4$ (111), Co_3WO_8 (001), Co_3WO_8 (101), Co_3WO_8 (110), $TiWO_4$ (011), $TiWO_4$ (100), and $TiWO_4$ (101). The catalytic activity of $CoWO_4$ in the oxygen evolution reaction (OER) and oxygen reduction reaction (ORR) has been thoroughly studied. Research has successfully created cube-shaped $CoWO_4$ nanoparticles, exploring their dual electro-catalytic roles in redox processes involving water. These $CoWO_4$ nano-cubes demonstrated exceptionally low overpotentials for ORR and OER, suggesting that they could be a more affordable option for noble electrode materials.
- Because it shows how reactive a catalyst is, the density of states (DOS) is very important. The increased availability of electron energy states over hole energy states across all surfaces, especially in the conduction band, increases the probability of improved conductivity, faster electron transfers kinetics, and enhanced catalytic activity during electrochemical reactions in fuel cells.
- $CoWO_4$ (011), $TiWO_4$ (100), and $TiWO_4$ (101) have relatively small band gaps or surfaces that facilitate easier electron mobility between the valence and conduction bands, indicating their potential applications as HOR and ORR. Similarly, Co_3WO_8 (001), Co_3WO_8 (101), and Co_3WO_8 (110) exhibit similar characteristics. This increased conductivity, combined with the surfaces' electrocatalytic surface properties, can result in more effective electron transfer, which can raise current and improve cell output. Using low activation energy may accelerate these reactions and increase the cell's output, as the narrow band gap influences the ease of electron stimulation.
- All of these surfaces successfully adsorbed both hydrogen and oxygen, and each reaction occurred independently. With three reaction sites on a 2×2 supercell surface and an adsorption energy of $-1{,}55$ Kcal/mol, $CoWO_4$ (011) is the most stable surface for hydrogen in $CoWO_4$. $CoWO_4$ (111) is the most stable surface for oxygen. It has three reaction sites on a 2×2 supercell surface and an adsorption energy of -22.12 Kcal/mol. At -1.34 Kcal/mol, Co_3WO_8 (001) is the most stable surface for hydrogen in Co_3WO_8. It has two reaction sites on a 2×2 supercell surface. Co_3WO_8 (001) is the most stable oxygen surface because it has two reaction sites on a 2×2 supercell surface and an adsorption energy of -21.99 Kcal/mol. $TiWO_4$ (011), which has three reaction sites on a 2×2 supercell surface with an adsorption energy of -1.40 kcal/mol, is the most stable surface for hydrogen in $TiWO_4$. $TiWO_4$ (101) is

the oxygen surface that is the most stable, with three reaction sites on a 2 × 2 supercell surface and an adsorption energy of −23.00 kcal/mol.

- Acquisition of evidence-based insights into the complexities of catalyst development, surface reactions of catalysts, electronic properties, and stability of the novel electrocatalysts. Insufficient comprehension of surface atoms on a catalyst poses significant challenges in determining the appropriate catalyst loading and achieving an acceptable particle size distribution. Understanding the surface atoms allows us to have a more profound understanding of their electrochemical characteristics, reactivity, and durability, which would advance fuel cell commercialization. These data can also be extrapolated to other catalyst systems.

2. Background

Few investigations have been conducted on $CoWO_4$ utilizing Density Functional Theory (DFT), with an emphasis on its electrical properties and prospective applications in supercapacitors for energy storage. $CoWO_4$ exhibits semiconductor behaviour with a conductivity behaviour transition at 750 K, suggesting applications in electronic devices. Despite limited research on its use in fuel cells and its potential in energy conversion reactions, further study is necessary to fully realize its potential [5,6]. There isn't much research on Co_3WO_8, especially in specialized studies that concentrate on its electrical and structural characteristics. Data from the Material Project provides insights that point to its potential as a catalyst, particularly for fuel cell applications. Nevertheless, more investigation is required to completely comprehend and enhance its catalytic action. To completely comprehend and exploit $TiWO_4$'s catalytic properties, more research is necessary, as there is currently a dearth of comprehensive knowledge committed to this compound alone. Improving its performance, robustness, and scalability are crucial prerequisites for its potential incorporation into fuel cell systems. Research indicates that Density Functional Theory (DFT) is essential for comprehending energy-related electrochemical reactions and improves our understanding of these processes [7,8]. It solves intricate issues that are difficult to resolve through experimental study, making it possible to compute adsorption energies and molecular geometries pertinent to catalyst materials used in fuel cells (FCs). DFT simulations help anticipate electrocatalyst properties and material design for enhanced fuel cell performance by offering insights into catalyst-gas interactions, stability, and catalytic activity [9].

3. Data Description

As can be observed in Fig. 1, $CoWO_4$ is a structure produced from zeta iron carbide that forms a monoclinic Pc group during crystallization. The tungsten ions (W^{6+}) in this structure form bonds with six oxygen ions (O^{2-}) to form octahedral forms known as WO_6 octahedral. Eight CoO_6 octahedral join the octahedral at their corners, while two extra WO_6 octahedral connect them along their edges. The octahedral show some distortion. The compound Co_3WO_8, which is part of the hexagonal $P6_3mc$ space group, has a crystal structure generated from beta Vanadium nitride, as seen in Fig. 2. The WO_6 octahedral are formed in this configuration when six O^{2-} atoms are coordinated with W^{4+}. These octahedral are symmetrical, sharing three sides and six corners with three other octahedral of the same CoO_6.

As demonstrated in Fig. 3, $TiWO_4$ is a hydrophilite-derived structure that crystallizes into a monoclinic P2/m space group. There are two distinct Ti_3O_4 sites in the structure. Each Ti^{4+} combines with six oxygen ions (O^{2-}) in the first Ti^{4+} site to form TiO_6 octahedral. These octahedral are connected to two additional TiO_6 octahedral structures by their edges, and they share corners with four further TiO_6 octahedral and four WO_6 octahedral. Table 1 displays a variety of energy characteristics, including the energy change upon adsorption (dEads/dNi), total energy (TE), adsorption energy (AE), rigid adsorption energy (RAE), and deformation energy (DE). It is evident from Table 1's negative energies that H_2 adsorbs spontaneously on all surfaces, releasing

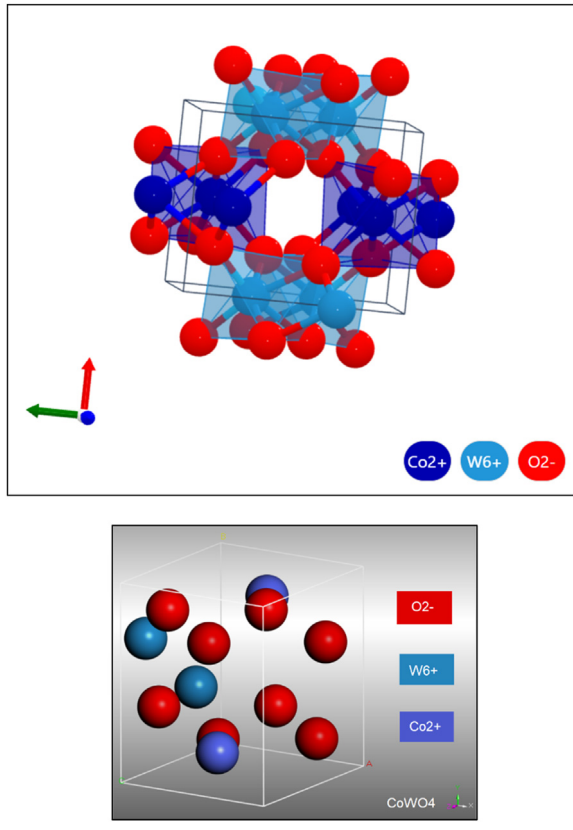

Fig. 1. Crystallographic structure of $CoWO_4$.

Table 1
Adsorption energies for H_2 adsorbed onto $CoWO_4$.

Structures	No. of sites	Total energy	Adsorption energy	Rigid adsorption energy	Deformation energy	H_2 : dEad/dNi
$CoWO_4$ (011)	1	−1.06631217	−1.55195814	−1.06633077	−0.48562737	−1.55195814
	2	−0.83337034	−1.31901631	−0.83337293	−0.48564338	−1.31901631
	3	−0.63265821	−1.11830417	−0.63266167	−0.48564250	−1.11830417
$CoWO_4$ (100)	1	−0.65036659	−1.13601256	−0.65036659	−0.48564596	−1.13601256
$CoWO_4$ (111)	1	−1.01755086	−1.50319683	−1.01755249	−0.48564433	−1.50319683
	2	−0.79810062	−1.28374659	−0.79821160	−0.48553499	−1.28374659
	3	−0.55850851	−1.04415448	−0.58082016	−0.46333432	−1.04415448

energy in the process. This indicates that $CoWO_4$ (011), $CoWO_4$ (100), and $CoWO_4$ (111) surfaces can all absorb H_2.

The negative values for these parameters in Table 2 demonstrate the spontaneous nature of the adsorption process. Specifically, Table 2 indicates that interactions between surfaces and O_2 adsorbates liberate energy, as indicated by the negative values for TE, AE, RAE, and DE. This shows that O_2 can adsorb onto the surfaces of $CoWO_4$ (011), $CoWO_4$ (100), and $CoWO_4$ (111) in more detail. The negative values observed across several energy parameters, which represent the favourability and strength of the contact between the oxygen molecules and the surfaces, emphasize the adsorption capacity of the relevant $CoWO_4$ surfaces. The adsorption energy results in

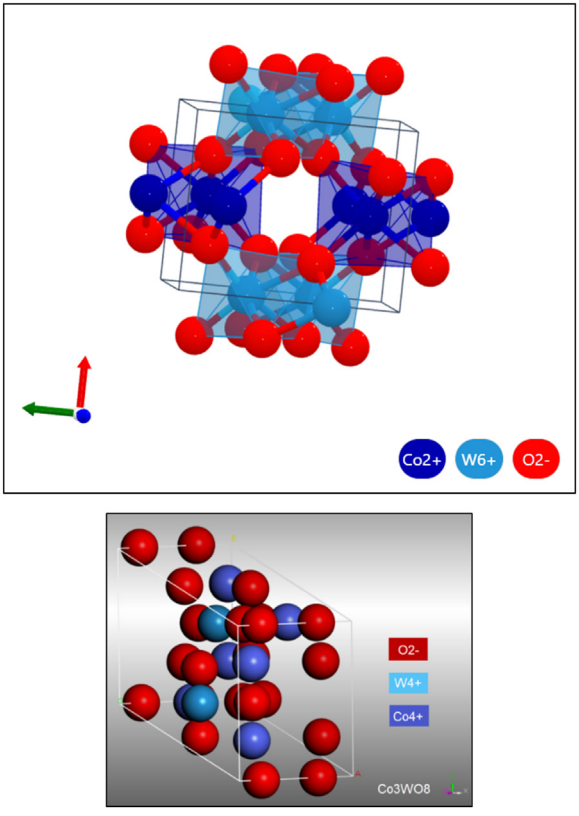

Fig. 2. Crystallographic structure of Co_3WO_8.

Table 2
Adsorption energies for O_2 adsorbed onto $CoWO_4$.

Structures	No. of sites	Total energy	Adsorption energy	Rigid adsorption energy	Deformation energy	O_2 : dEad/dNi
$CoWO_4$ (011)	1	−1.22635872	−21.95241580	−1.22636213	−20.72605367	−21.95241580
	2	−1.02512017	−21.75117725	−1.02524428	−20.72593297	−21.75117725
	3	−0.81931989	−21.54537697	−0.81932037	−20.72605660	−21.54537697
	4	−0.44056689	−21.16662397	−0.44059066	−20.72603332	−21.16662397
$CoWO_4$ (100)	1	−0.91223121	−21.63828829	−0.91223136	−20.72605693	−21.63828829
$CoWO_4$ (111)	1	−1.40158518	−22.12764227	−1.40158660	−20.72605566	−22.12764227
	2	−1.20034872	−21.92640580	−1.20257463	−20.72383117	−21.92640580
	3	−0.96322633	−21.68928341	−0.96690981	−20.72237361	−21.68928341

surface reaction analysis of catalysts are greater than the deformation energy values, suggesting that the O_2 molecule adsorption onto the catalytic surface is more energetically advantageous than any potential structural modifications during adsorption.

Tables 3 and 4 display the various surface configurations of Co_3WO_8 (001), Co_3WO_8 (101), and Co_3WO_8 (110) following H_2 and O_2 adsorption. On the (101) surface, one H_2 adoption site was occupied, in contrast to the density of states' initial prediction that multiple accessible adsorption sites were present. Table 3 displays various energy measures, including adsorption energy (AE), total energy (TE), rigid adsorption energy (RAE), deformation energy (DE), and the energy change following adsorption (dEads/dNi). The H_2 adsorption capacity onto Co_3WO_8 (001),

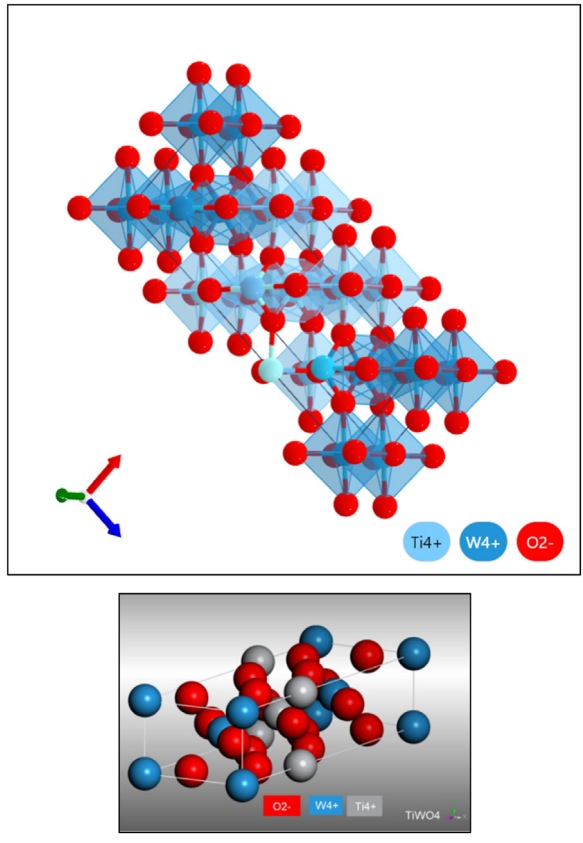

Fig. 3. Crystallographic structure of $TiWO_4$.

Table 3
Adsorption energies for H_2 adsorbed onto Co_3WO_8.

Structures	No. of sites	Total energy	Adsorption energy	Rigid adsorption energy	Deformation energy	H_2 : dEad/dNi
Co_3WO_8 (001)	1	−0.91126455	−1.39691052	−0.91126663	−0.48564389	−1.39691052
	2	−0.70472169	−1.19036766	−0.70686768	−0.48349997	−1.19036766
Co_3WO_8 (101)	1	−0.85869210	−1.34433807	−0.85869668	−0.48564139	−1.34433807
	2	−0.65195598	−1.13760195	−0.65195599	−0.48564596	−1.13760195
Co_3WO_8 (110)	1	−0.88140275	−1.36704872	−0.88140964	−0.48563908	−1.36704872
	2	−0.67509559	−1.16074156	−0.67542431	−0.48531725	−1.16074156

Table 4
Adsorption energies for O_2 adsorbed onto Co_3WO_8.

Structures	No. of sites	Total energy	Adsorption energy	Rigid adsorption energy	Deformation energy	O_2 : dEad/dNi
Co_3WO_8 (001)	1	−1.26206132	−21.98811840	−1.26206253	−20.72605587	−21.98811840
	2	−1.02961961	−21.75567670	−1.02962813	−20.72604857	−21.75567670
	3	−0.50360674	−21.22966382	−0.50372526	−20.72593857	−21.22966382
Co_3WO_8 (101)	1	−1.15347278	−21.87952987	−1.15347344	−20.72605643	−21.87952987
	2	−0.93887354	−21.66493063	−0.93887570	−20.72605493	−21.66493063
	3	−0.58386233	−21.30991942	−0.58390661	−20.72601281	−21.30991942
Co_3WO_8 (110)	1	−1,11,830,634	−21,84,436,342	−1,11,830,642	−20,72,605,700	−21,84,436,342
	2	−0,88,398,884	−21,61,004,592	−0,88,401,506	−20,72,603,086	−21,61,004,592

Table 5
Adsorption energies for H_2 adsorbed onto $TiWO_4$.

Structures	No. of sites	Total energy	Adsorption energy	Rigid adsorption energy	Deformation energy	H_2 : dEad/dNi
$TiWO_4$ (011)	1	−0.91536014	−1.40100610	−0.91536463	−0.48564147	−1.40100610
	2	−0.81480518	−1.30045115	−0.81486899	−0.48558216	−1.30045115
	3	−0.60808223	−1.09372820	−0.61095999	−0.48276820	−1.09372820
	4	−0.39965222	−0.88529819	−0.39968761	−0.48561057	−0.88529819
$TiWO_4$ (100)	1	−0.94005766	−1.42570363	−0.94005815	−0.48564548	−1.42570363
	2	−0.75596488	−1.24161085	−0.75596534	−0.48564551	−1.24161085
	3	−0.70383420	−1.18948017	−0.71466400	−0.47481617	−1.18948017
	4	−0.49733145	−0.98297742	−0.49735454	−0.48562288	−0.98297742
$TiWO_4$ (101)	1	−1.05612572	−1.54177169	−1.05612573	−0.48564596	−1.54177169
	2	−0.78950836	−1.27515433	−0.78950902	−0.48564531	−1.27515433
	3	−0.64205506	−1.12770103	−0.64205515	−0.48564588	−1.12770103
	4	−0.43844636	−0.92409233	−0.43844638	−0.48564595	−0.92409233

Table 6
Adsorption energies for O_2 adsorbed onto $TiWO_4$.

Structures	No. of sites	Total energy	Adsorption energy	Rigid adsorption energy	Deformation energy	O_2 : dEad/dNi
$TiWO_4$ (011)	1	−1.20818760	−21.93424468	−1.20818801	−20.72605667	−21.93424468
	2	−1.01250228	−21.73855936	−1.01250303	−20.72605634	−21.73855936
	3	−0.89429533	−21.62035241	−0.91874715	−20.70160526	−21.62035241
	4	−0.80830829	−21.53436538	−0.80831442	−20.72605095	−21.53436538
	5	−0.58785356	−21.31391064	−0.58785356	−20.72605708	−21.31391064
$TiWO_4$ (100)	1	−1.27229962	−21.99835671	−1.27229983	−20.72605688	−21.99835671
	2	−1.13977460	−21.86583169	−1.13977929	−20.72605240	−21.86583169
	3	−1.05061026	−21.77666734	−1.05157655	−20.72509080	−21.77666734
	4	−0.70844003	−21.43449711	−0.70847550	−20.72602161	−21.43449711
$TiWO_4$ (101)	1	−1.50140317	−22.22746025	−1.50140340	−20.72605686	−22.22746025
	2	−1.29722214	−22.02327922	−1.29723635	−20.72604287	−22.02327922
	3	−1.09640041	−21.82245750	−1.09640455	−20.72605295	−21.82245750
	4	−0.90553061	−21.63158769	−0.90553061	−20.72605708	−21.63158769
	5	−0.84554007	−21.57159716	−0.84554014	−20.72605702	−21.57159716
	6	−0.65422514	−21.38028222	−0.65810465	−20.72217758	−21.38028222

Co_3WO_8 (101), and Co_3WO_8 (110) surfaces is confirmed by Table 3's negative energies, which also show that H_2 is spontaneously adsorbed on all surfaces. Energy is released during this process. The different surfaces configurations of Co_3WO_8 (001), Co_3WO_8 (101), and Co_3WO_8 (110) following O_2 adsorption are listed in Table 4. Initially, the density of states predicted that there would be a greater number of accessible adsorption sites. Various energy measurements, including as total energy, electrostatic energy, van der Waals energy, average total energy, and intermolecular energy, are applied to optimize the surface interactions between these surfaces and oxygen molecules. The found negative values for all these energy components in Table 4 demonstrate the spontaneous nature of the adsorption process. The data, specifically the negative values of TE, AE, RAE, and DE, demonstrated the release of energy during the interactions between the surfaces and O_2 adsorbates. This suggests that O_2 can adsorb onto surfaces of Co_3WO_8 (001), Co_3WO_8 (101), and Co_3WO_8 (110).

Tables 5 and 6 present different combinations of these surfaces when H_2 and O_2 are adsorbed, respectively, revealing energy configurations for the adsorbates. $TiWO_4$ (011), $TiWO_4$ (100), and $TiWO_4$ (101) surfaces exhibited optimized interactions with hydrogen molecules, exhibiting a range of energy metrics including total energy, intermolecular energy, Van der Waals energy, average total energy, and electrostatic energy. The $TiWO_4$ (011), $TiWO_4$ (100), and $TiWO_4$ (101) surfaces all showed increased adsorption sites, confirming the Density of States (DOS) initial suggestion of enhanced adsorption site availability. The rigid adsorption energy (RAE), total

energy (TE), deformation energy (DE), adsorption energy (AE), and energy change after adsorption (dEads/dNi) are listed in Table 5. Negative energies on all surfaces validate the spontaneous H_2 adsorption and energy release processes.

DFT calculations may produce erroneous or unrealistic findings if convergence is not achieved, which could result in incorrect predictions about the behaviour and performance of the catalyst. The systems attained the lowest energy configuration (Figs. 4–9) by CASTEP and Dmol3 geometry optimizations of $CoWO_4$ (011), $CoWO_4$ (100), and $CoWO_4$ (111). Optimization convergence was carried out and forces acting on the atoms were minimized. By using CASTEP and Dmol3 geometry optimizations for Co_3WO_8 (001), Co_3WO_8 (101), and Co_3WO_8 (110), the systems attained the lowest energy configuration (Figs. 10–15). Optimization convergence was achieved and forces acting on the atoms were minimized. $TiWO_4$ is unique in its chemical makeup. In addition to including titanium, its chemical composition noticeably excludes cobalt. By decreasing stresses on atoms and achieving the lowest energy configuration (shown in Figs. 16–21) by CASTEP and Dmol3 geometry optimizations of $TiWO_4$ (011), $TiWO_4$ (100), and $TiWO_4$ (101), convergence was enabled to ensure reliable results.

When optimizing a molecule's geometry with density functional theory (DFT), the goal is to find the lowest ground state energy feasible while simultaneously creating the most stable structure possible by shifting the atoms around. For lattice optimizations, the stress energy per atom is tracked, in addition to up to four other quantities: energy change, Cartesian gradients, Cartesian step size, and convergence. One common use case for CASTEP is geometry optimization. Optimization of CASTEP geometry relies on bringing the magnitude of computed stresses and forces down to levels below specified convergence tolerances. There is enormous significance and relevance in Figs. 4–21.

4. Experimental Design, Materials and Methods

DMol3 simulations were executed during the geometry optimization phase with great precision. To achieve this, we used periodic supercells in conjunction with the Generalized Gradient Approximation (GGA) and the Perdew–Burke–Ernzerhof (PBE) exchange-correlation functional with spin-polarized analysis. We ensured the computational accuracy by establishing extensive convergence criteria. A maximum force tolerance of 0.002 Hartree per Ångstrom (Ha/é) and a kinetic energy cutoff of 100 eV were used during form optimization [10]. The self-consistent field (SCF) cycle had strict $1.0e^{-6}$ convergence requirements. The thresholds for energy change, maximum force, and displacement between optimization cycles were $1.0e^{-5}$ Hartree (Ha), 0.02 Ha/é, and 0.05 Å, respectively. The radii of the self-consistent field (SCF) and the rapid multipole technique (FMS) were considered to guarantee accuracy in the simulations. To prevent periodic images from interacting, a 20 Å vacuum interval was used to divide the slab layers. A smearing factor of 0.05 Ha, a self-consistent loop energy of 10^6, and a global orbital cut-off radius of approximately 5.0 Å were the critical parameters. In a study comparing using the CASTEP module, geometric optimization was followed for the following compounds: $CoWO_4$ (011), $CoWO_4$ (100), $CoWO_4$ (111), Co_3WO_8 (001), Co_3WO_8 (101), Co_3WO_8 (011), $TiWO_4$ (100), $TiWO_4$ (101), and $TiWO_4$ (110). The Generalized Gradient Approximation (GGA) formula is based on the Exchange-Correlation Energy Functional ($Exc[\rho]$), which changes based on the electron density $\rho(r)$. Most of the time, we express the GGA functional using the local electron density and associated gradients.

Based on the ideas described earlier, we use Materials Studio to model and simulate the Ti-Co-W oxide structures. The software package was developed and distributed by BIOVIA, a company that focuses on research tools for areas such as computational chemistry, quantum mechanics, molecular dynamics simulations, bioinformatics, and chemoinformatics. A wide range of materials, including catalysts, polymers, nanotubes, metals, ceramics, and more, can be subjected to in-depth investigations using the Material Studio application. A large number of researchers have made use of this instrument to overcome obstacles in catalyst and fuel cell development. A number of computer modules developed specifically for use in material property simulations

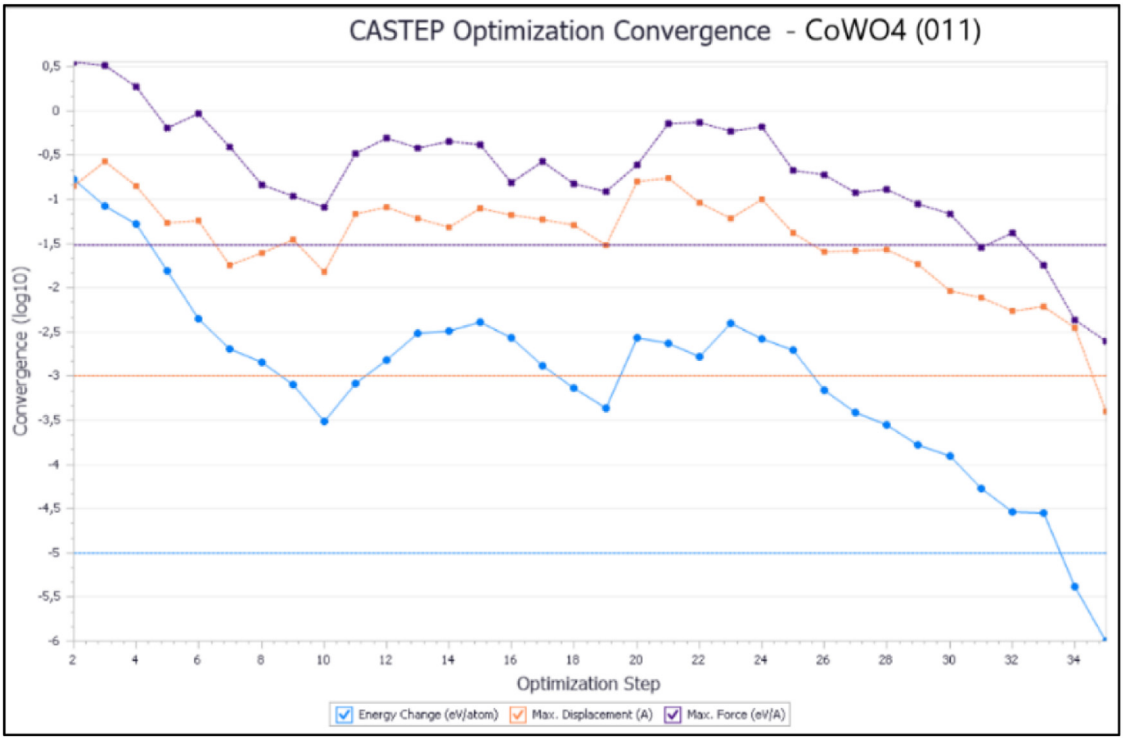

Fig. 4. Optimization convergence of $CoWO_4$ (011) surface with respects to CASTEP module.

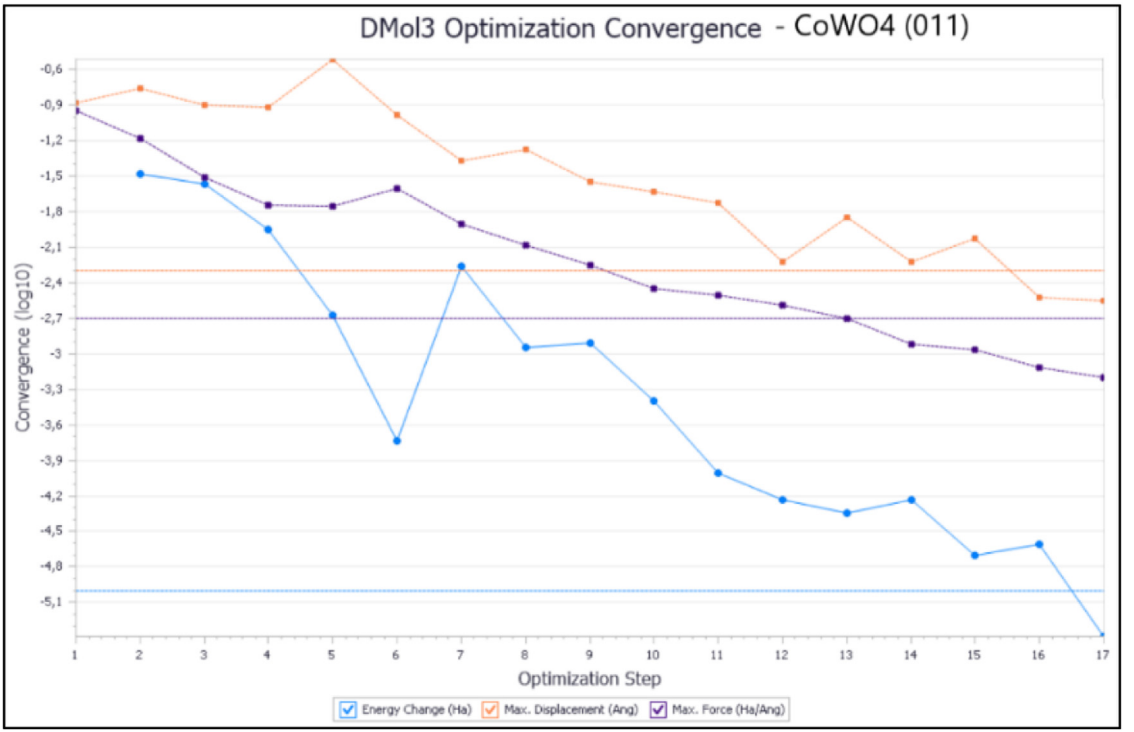

Fig. 5. Optimization convergence of $CoWO_4$ (011) surface with respects to Dmol3 module.

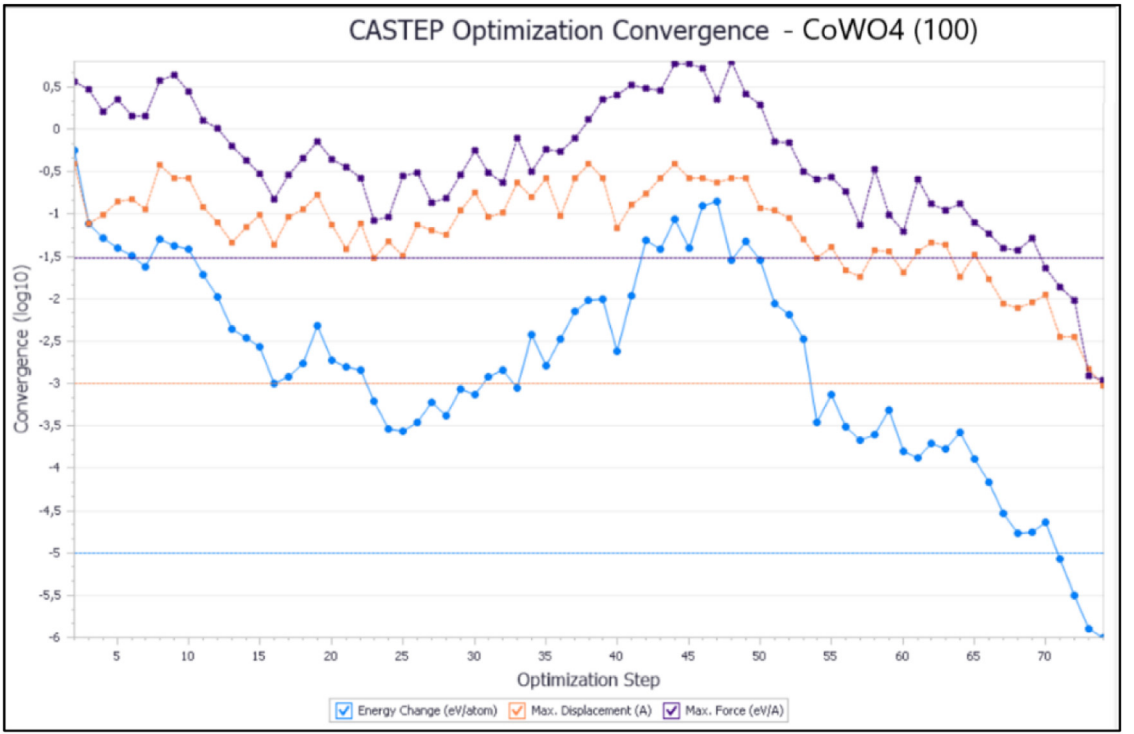

Fig. 6. Optimization convergence of $CoWO_4$ (100) surface with respects to CASTEP module.

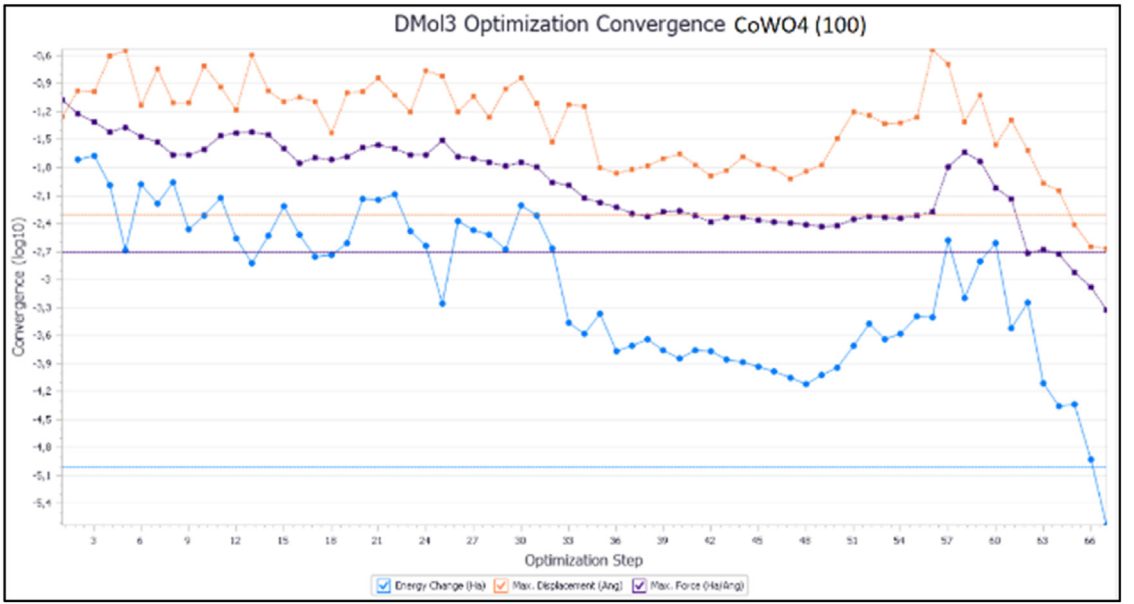

Fig. 7. Optimization convergence of $CoWO_4$ (100) surface with respects to Dmol3 module.

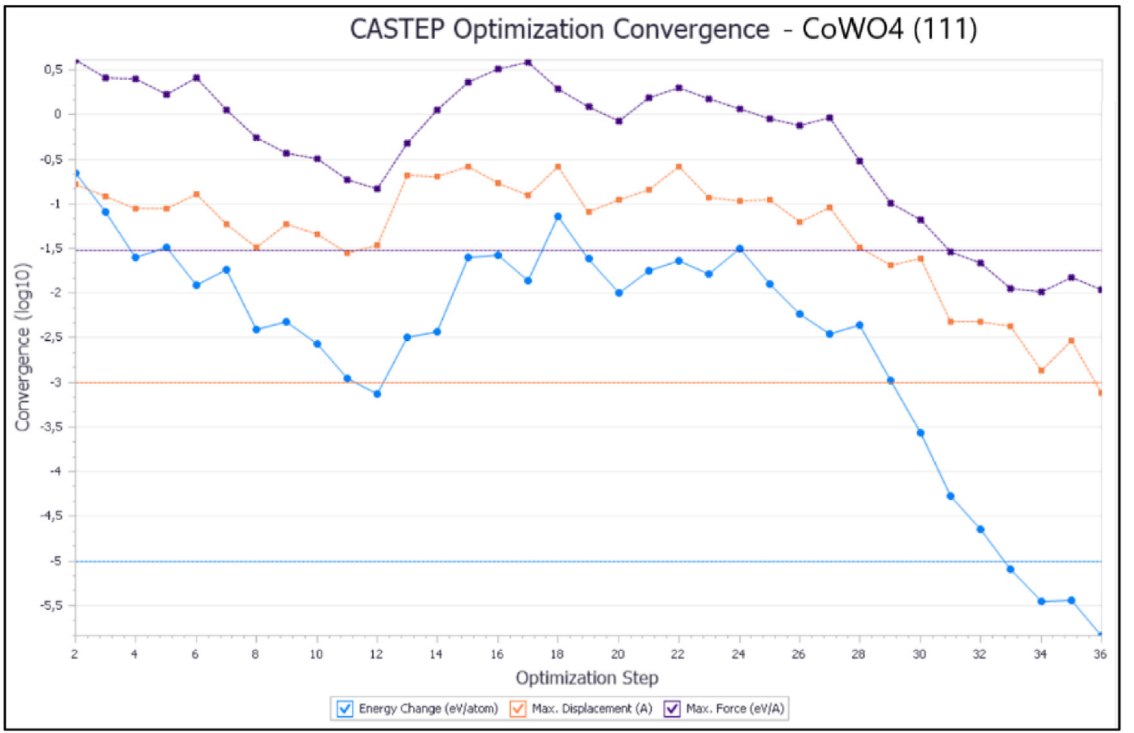

Fig. 8. Optimization convergence of $CoWO_4$ (111) surface with respects to CASTEP module.

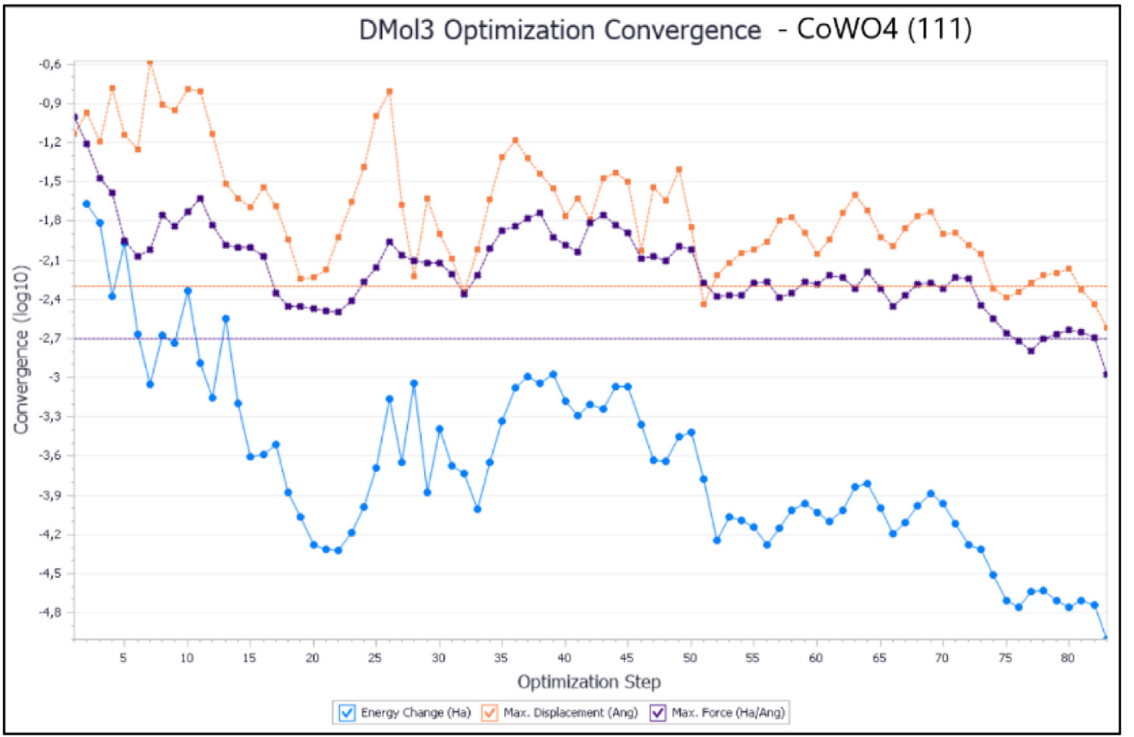

Fig. 9. Optimization convergence of $CoWO_4$ (111) surface with respects to Dmol3 module.

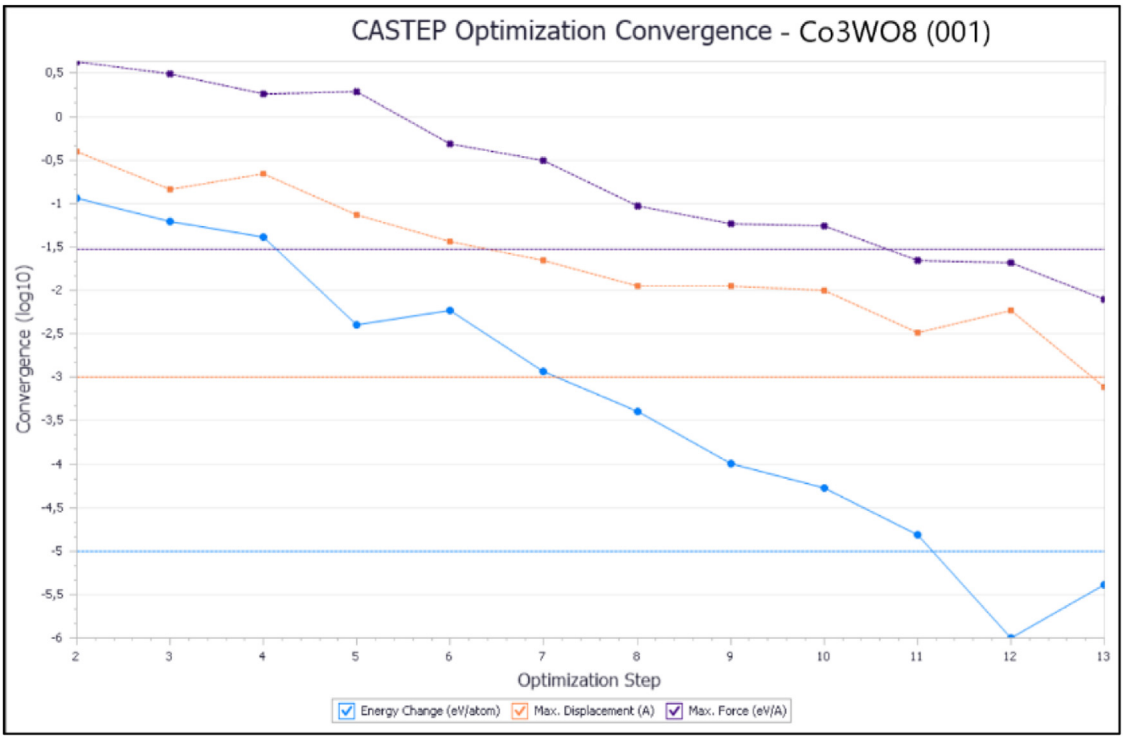

Fig. 10. Optimization convergence of Co_3WO_8 (001) surface with respects to CASTEP module.

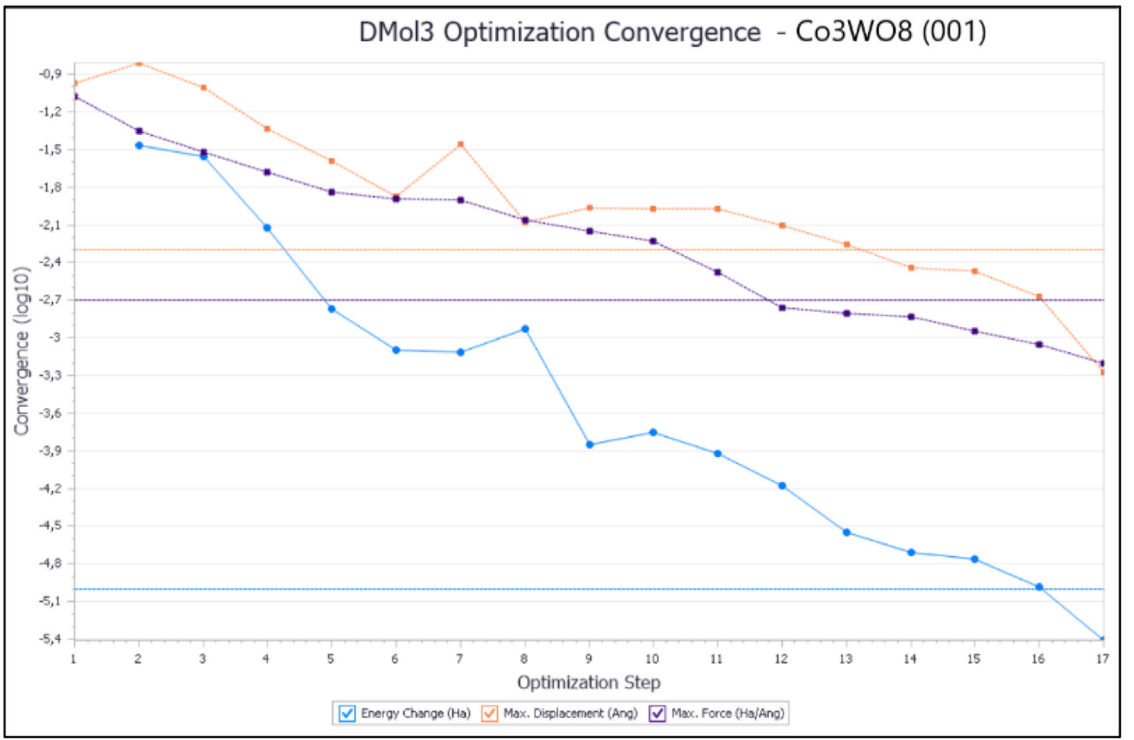

Fig. 11. Optimization convergence of Co_3WO_8 (001) surface with respects to DMOL3 module.

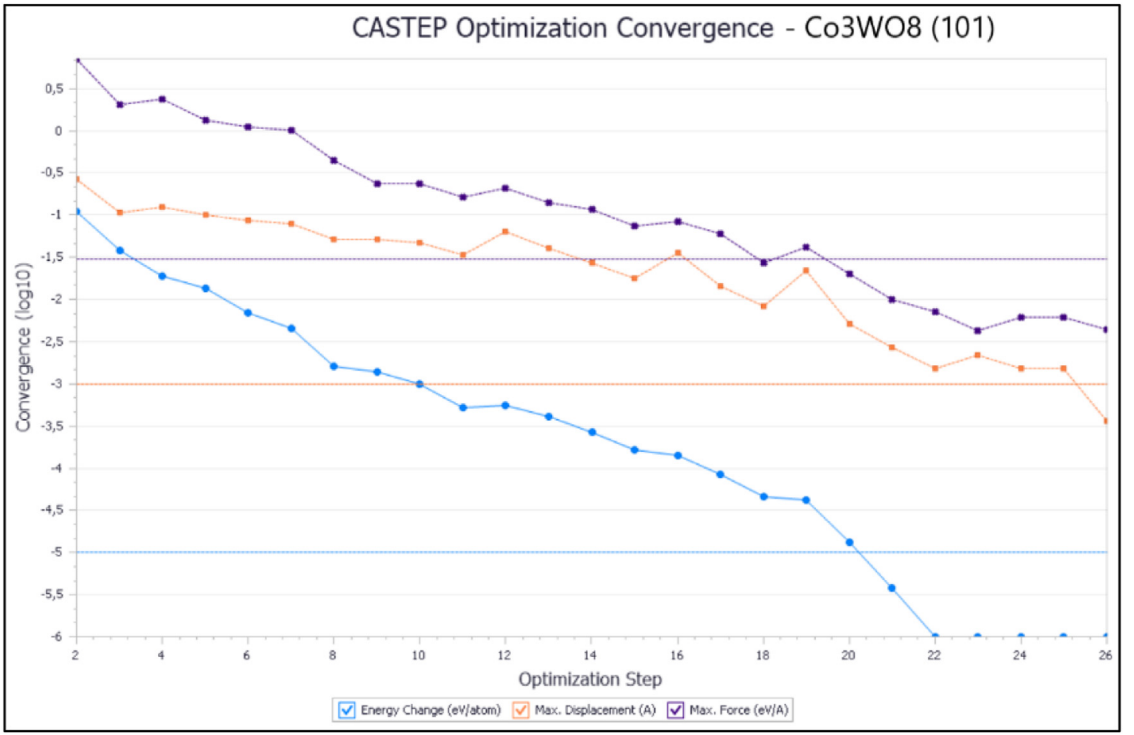

Fig. 12. Optimization convergence of Co_3WO_8 (101) surface with respects to CASTEP module.

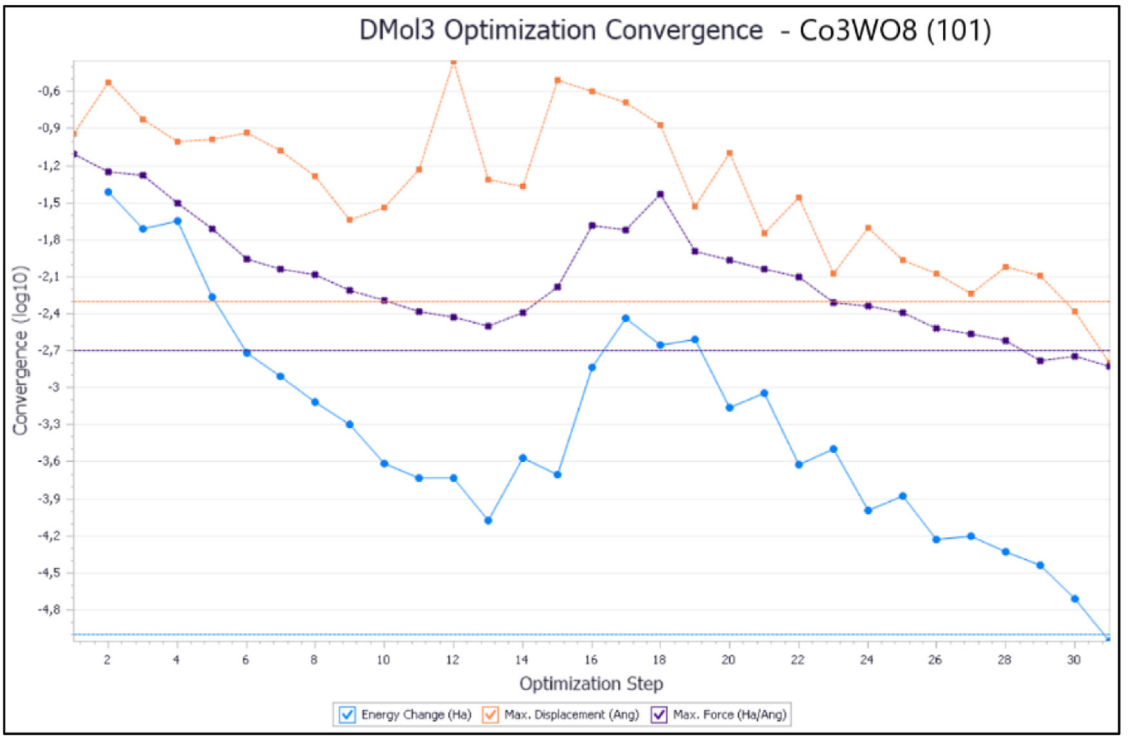

Fig. 13. Optimization convergence of Co_3WO_8 (101) surface with respects to DMOL3 module.

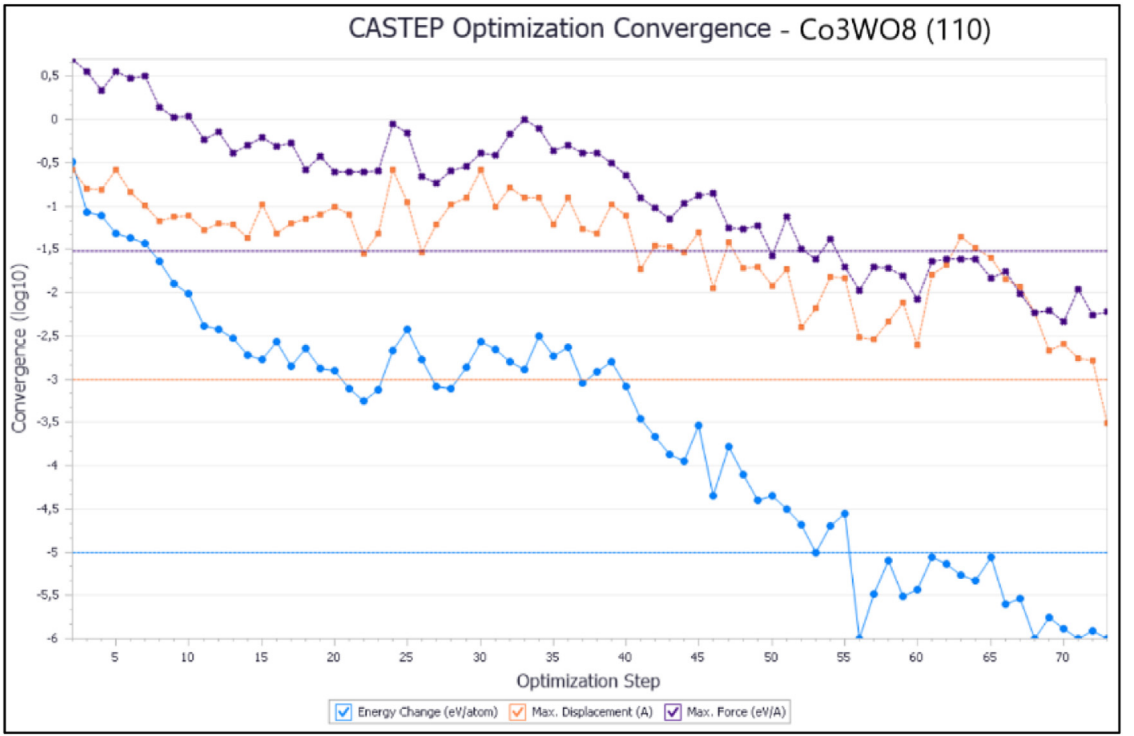

Fig. 14. Optimization convergence of Co_3WO_8 (110) surface with respects to CASTEP module.

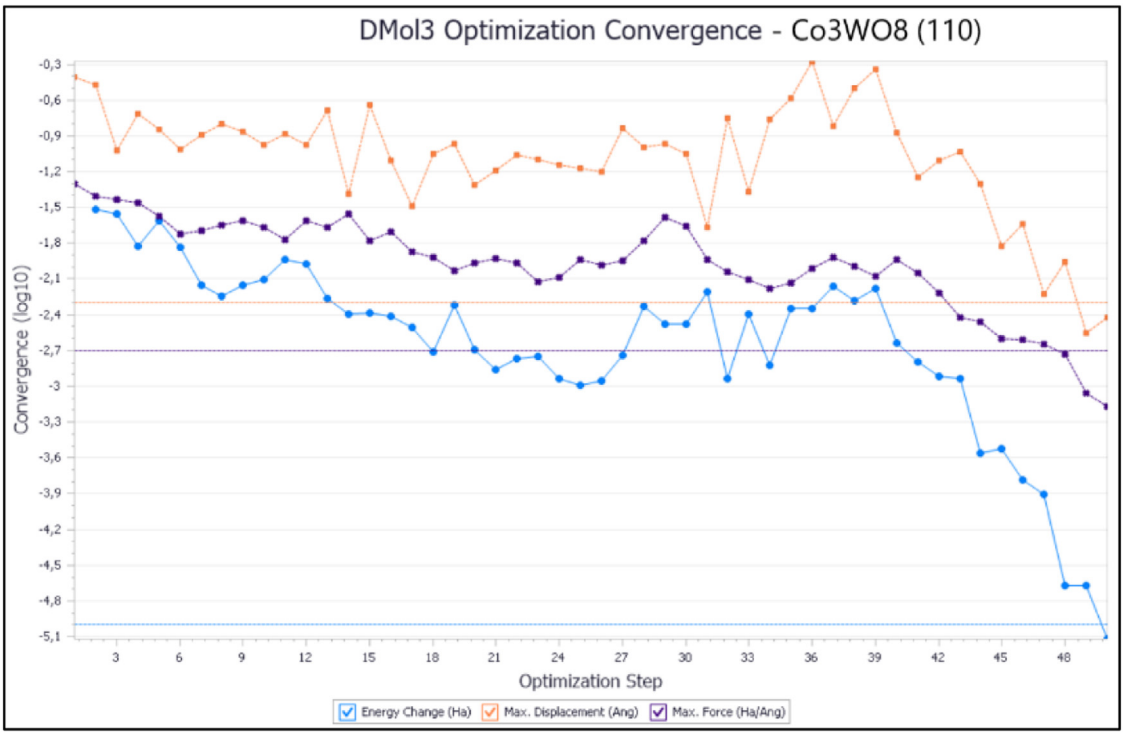

Fig. 15. Optimization convergence of Co_3WO_8 (110) surface with respects to DMOL3 module.

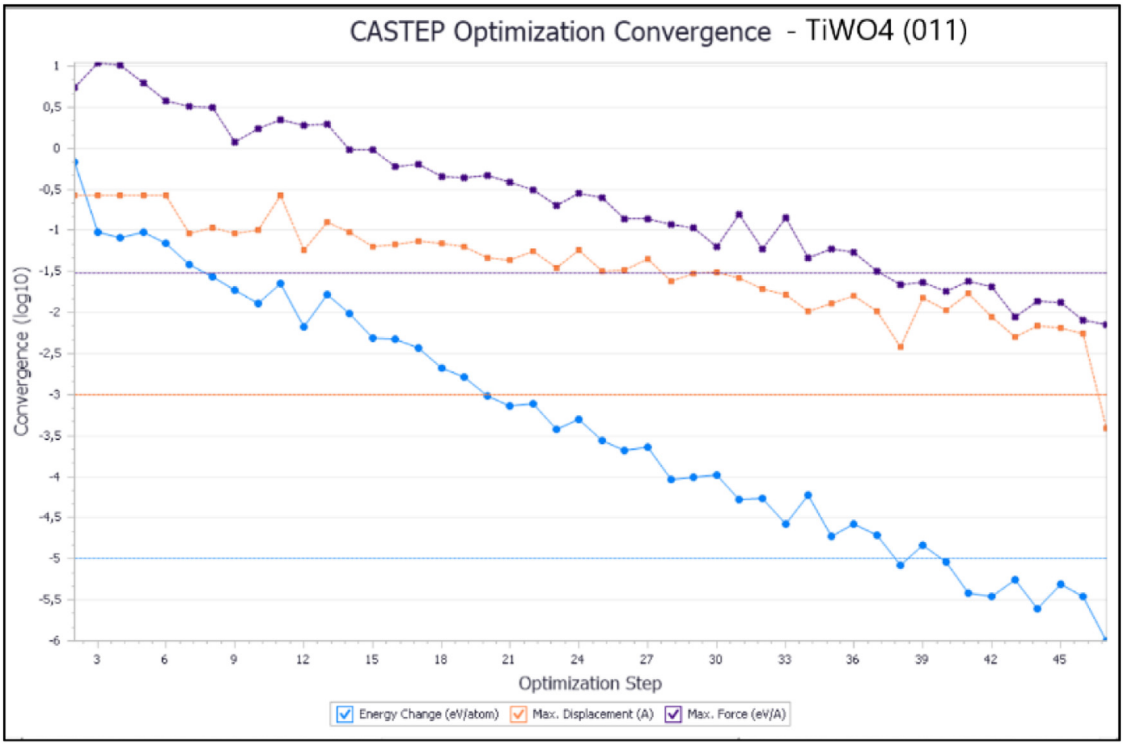

Fig. 16. Optimization convergence of $TiWO_4$ (011) surface with respects to CASTEP module.

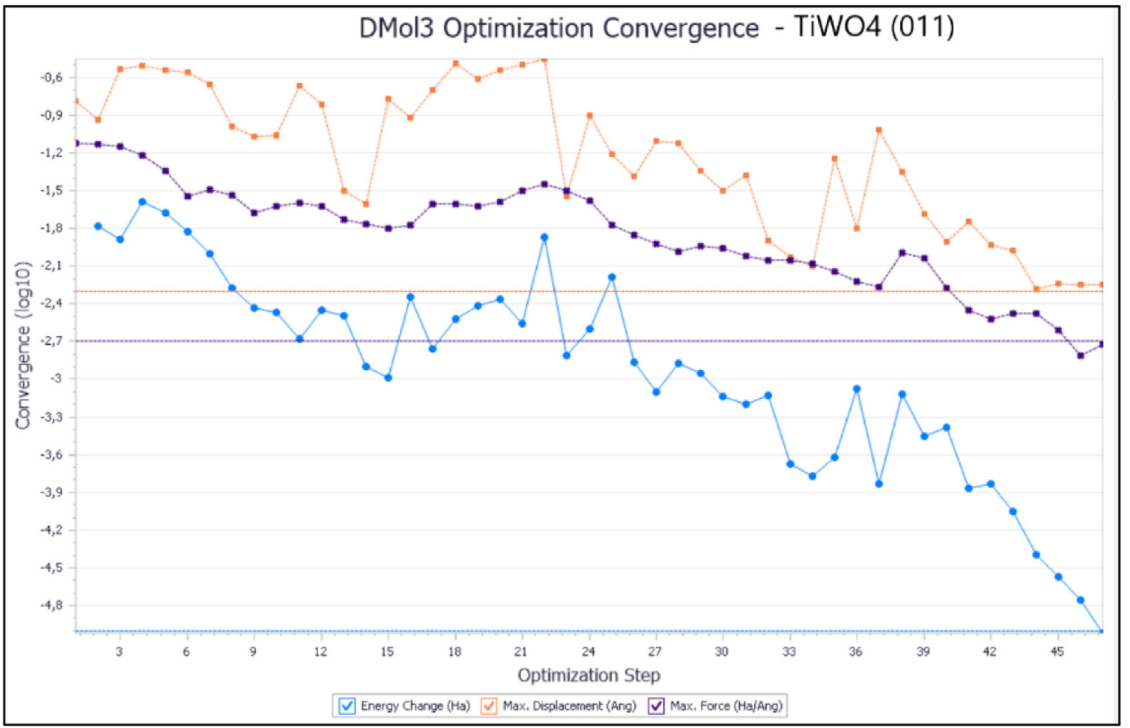

Fig. 17. Optimization convergence of $TiWO_4$ (011) surface with respects to DMol3 module.

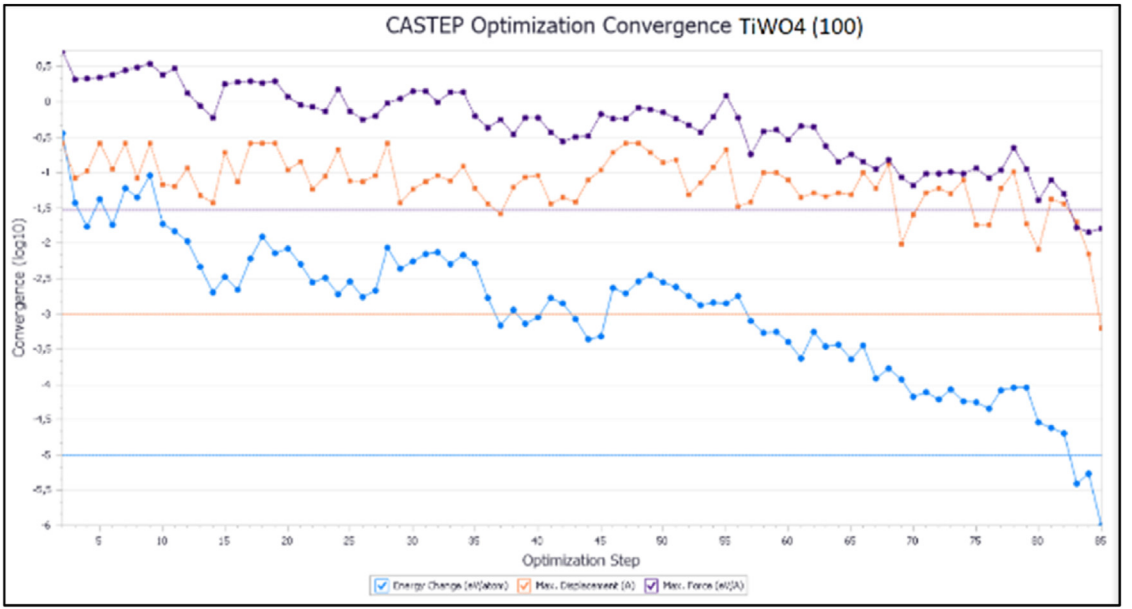

Fig. 18. Optimization convergence of $TiWO_4$ (100) surface with respects to CASTEP module.

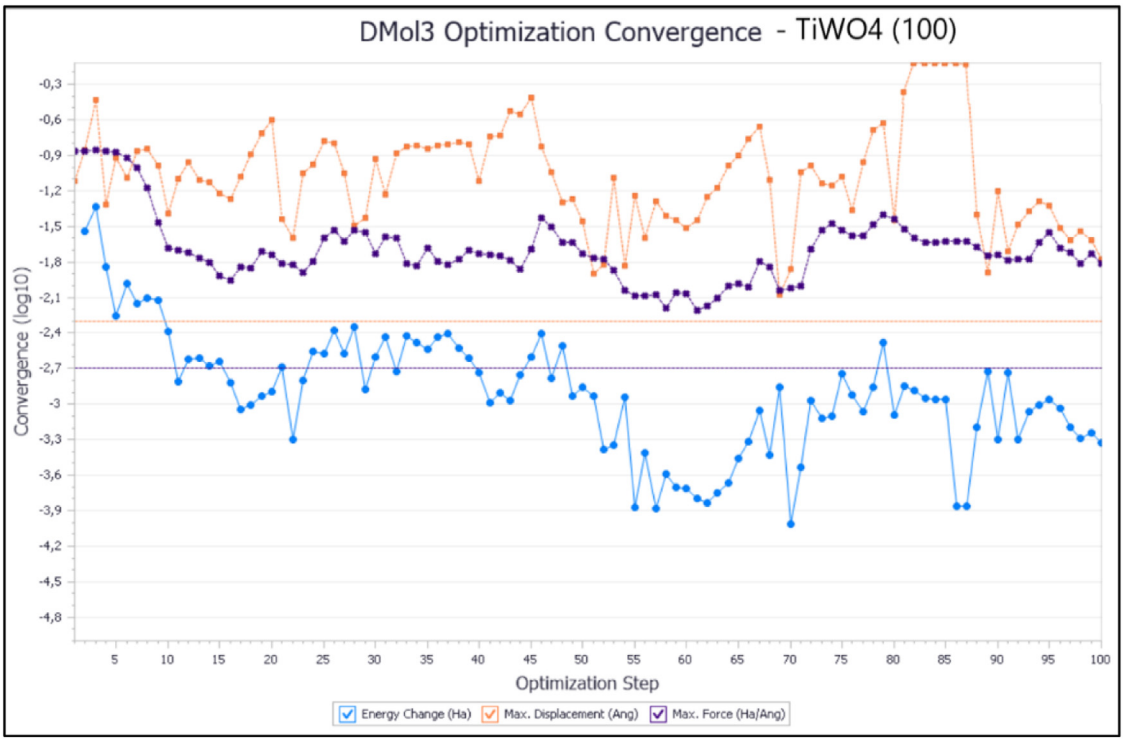

Fig. 19. Optimization convergence of $TiWO_4$ (100) surface with respects to DMol3 module.

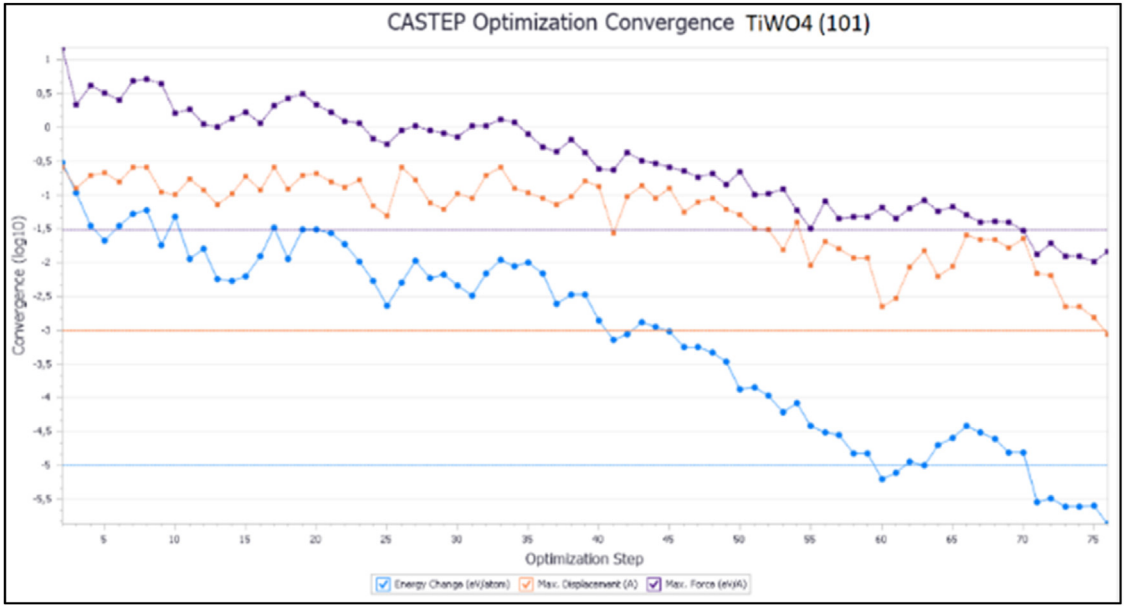

Fig. 20. Optimization convergence of $TiWO_4$ (101) surface with respects to Dmol3 module.

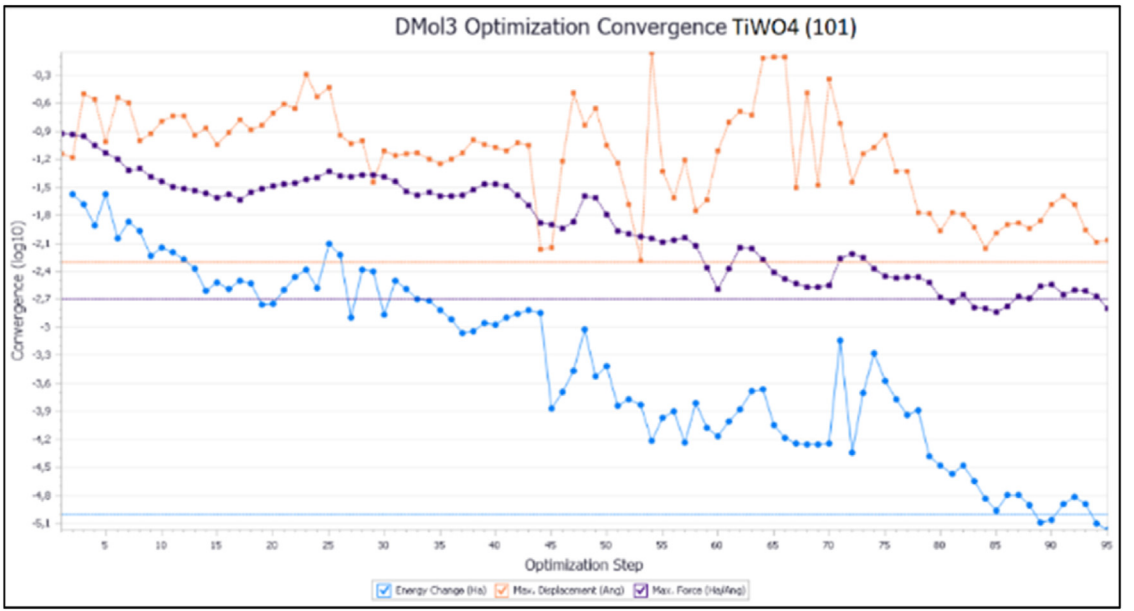

Fig. 21. Optimization convergence of $TiWO_4$ (101) surface with respects to Dmol3 module.

and predictive modelling are utilized in this study. Two important modules used are DMol3, which makes predictions about material characteristics, and CASTEP, which makes predictions about electrical, optical, and structural properties and allows comparisons with DMol3.

Many factors are considered in the computations of this study, including gas adsorption, density of states, population analysis, band structure, electron density, and gas density. Transition metal oxide density of states (DOS) is an important property to study for fuel cell catalysts, especially in the context of the oxygen reduction process (ORR). We can learn more about the bonding characteristics and structural composition of clusters of transition metal oxides by calculating their density of states (DOS). Because of their small atomic number, these clusters exhibit distinctive properties that are crucial to understanding their catalytic action [11]. The utilization of density functional theory (DFT) simulations has enabled the investigation of the functional role of transition metal oxides (TMOs) in relation to the oxygen reduction process (ORR). The particular objective of this modelling approach is to convey and understand the structural and electrical properties of reducible transition metal oxides. The area of fuel cell catalysts is greatly impacted by these oxides due to their central role in catalysis [12].

In particular, density-functional theory (DFT) simulations of transition metal oxide fuel cell catalysts are crucial research tools. This becomes even more apparent when you include demographic analysis. In order to understand the complex atomic and electronic properties of materials, it is necessary to do these computations [12]. A quantum mechanically-based computational method called density functional theory (DFT) has made it possible to study in detail how these transition metal oxides interact with other chemicals that are important for fuel cells.

Limitations

Not Applicable

Ethics Statement

The authors have read and follow the ethical requirements for publication in Data in Brief and confirming that the current work does not involve human subjects, animal experiments, or any data collected from social media platforms.

CRediT Author Statement

Olawale Samuel Fatoba: Conceptualization, Validation, Supervision, Conceptualization, Methodology, Validation, Writing – review & editing; **Salaminah Bonolo Boshoman**: Methodology, Validation, Software, Data curation, Conceptualization, Formal analysis, Writing – original draft.

Data availability

Data Related to the Catalytic Capabilities of Transition Metal Oxides for Energy Applications (Original data) (Mendeley Data)

Acknowledgements

The authors gratefully acknowledge the University of Johannesburg, the department of mechanical engineering, and CHPC for the collaborative research work. This research did not receive any specific grant from funding agencies in the public, commercial, or not-for-profit sectors.

Declaration of Competing Interest

The authors declare that they have no known competing financial interests or personal relationships that could have appeared to influence the work reported in this paper.

References

[1] S.B. Boshoman, O.S. Fatoba, O.O. Dada, T.C. Jen, Transition metal oxide catalytic abilities for fuel cell applications: density functional theory (DFT) studies, Mater. Today Commun. 39 (2024) 1–16 109125, doi:10.1016/j.mtcomm.2024.109125.
[2] S. Sharma, P. Kumar, R. Chandra, Introduction to Molecular Dynamics, Elsevier Inc., 2019, doi:10.1016/B978-0-12-816954-4.00001-2.
[3] X. Hu, X. Wang, T. Zhou, X. Chu, C. Xie, D. Zeng, Sensors and Actuators B : chemical Insight into highly selective dimethyl trisul fi de detection based on WO 3 nanorod bundles with exposed (002) facets, Sens. Actuators B. Chem. 305 (2020) 127538, doi:10.1016/j.snb.2019.127538.
[4] A. Baghban, S. Habibzadeh, F.Z. Ashtiani, Activity of transition metals in N-doped carbon Electrocatalysts for hydrogen evolution reaction : insight from quantum chemistry computations, Int. J. Energy Res. 46 (1) (2021) 1–9, doi:10.1002/er.7280.
[5] R. Senthil, Recent innovations in solar energy education and research towards sustainable energy development, Acta Innov. 2022 (42) (2022) 27–49, doi:10.32933/ActaInnovations.42.3.
[6] M.M. Farag, R.C. Bansal, Solar energy development in the GCC region–a review on recent progress and opportunities, Int. J. Model. Simul. 43 (5) (2022) 579–599, doi:10.1080/02286203.2022.2105785.
[7] W. Raza, K. Ahmad, Recent progress on perovskite-based solar cells, Perovskite Mater. Energy Environ. Appl. 44 (2022) 147–165, doi:10.1002/9781119763376.ch6.
[8] A. Digambar Singh, B. Yog Raj Sood, C. Deepak, Recent techno-economic potential and development of solar energy sector in India, IETE Tech. Rev. (Inst. Electron. Telecommun. Eng. India) 37 (3) (2022) 246–257, doi:10.1080/02564602.2019.1596043.
[9] D. Turner, M. Li, D. Grant, O. Ola, Recent enterprises in high-rate monolithic photo-electrochemical energy harvest and storage devices, Curr. Opin. Electrochem. 38 (2023), doi:10.1016/j.coelec.2023.101243.
[10] M.I. Sohail, et al., Environmental Application of Nanomaterials: a Promise to Sustainable Future, 87, 1st ed., Elsevier B.V, 2019, doi:10.1016/bs.coac.2019.10.002.
[11] Y.X. Zhao, X.L. Ding, Y.P. Ma, Z.C. Wang, S.G. He, Transition metal oxide clusters with character of oxygen-centered radical: a DFT study, Theor. Chem. Acc. 127 (5) (2010) 449–465, doi:10.1007/s00214-010-0732-8.
[12] A.B. Getsoian, A.T. Bell, The influence of functionals on density functional theory calculations of the properties of reducible transition metal oxide catalysts, J. Phys. Chem. C 117 (48) (2013) 25562–25578, doi:10.1021/jp409479h.